On the dopability of semiconductors and governing materials properties

Anuj Goyal,[†] Prashun Gorai,[†] Shashwat Anand,[‡] Eric S. Toberer,[†] G. Jeffrey Snyder,[‡] and Vladan Stevanović[*,†]

[†]*Colorado School of Mines, Golden, CO 80401, USA*

[‡]*Northwestern University, Evanston, IL, USA*

E-mail: vstevano@mines.edu

Supplementary Information

Cation vacancy

The n-type dopability metric, Eq. (9) in the main text, based only on cation vacancy is given as:

$$\delta\varepsilon_F^{(V_c)} = \bar{\varepsilon}_c - CBM + \frac{1}{N_c}(\bar{V}_c - V_\alpha) + \frac{1}{N_c}\Delta\mu_c, \quad (1)$$

Upgrading the model to account for the loss of N_c^s amount of electrons from the cation-s states ($\bar{\varepsilon}_c^s$) in the valence band of the compound to the reference phase, for systems like PbX and Bi_2X_3 (X = S, Se, Te). Also, assuming cation-rich conditions for the n-type doping ($\Delta\mu_c = 0$), changes Eq.(1) to:

$$\begin{aligned}
\delta\varepsilon_F^{(V_c)} &= \bar{\varepsilon}_c - CBM + \frac{N_c^s}{N_c}\big(\bar{\varepsilon}_c - \bar{\varepsilon}_c^s\big) + \frac{1}{N_c}(\bar{V}_c - V_\alpha), \\
\delta\varepsilon_F^{(V_c)} &= \big(1 + \frac{N_c^s}{N_c}\big)\bar{\varepsilon}_c - CBM - \frac{N_c^s}{N_c}\bar{\varepsilon}_c^s + \frac{1}{N_c}(\bar{V}_c - V_\alpha),
\end{aligned} \tag{2}$$

Using intrinsic material properties as proxies to replace the physically derived terms in Eq.(2). We approach by (1) fitting parameter $\times$ work function of the cation (W_c), $a \times W_c$, as a substitute for the $\big(1 + \frac{N_c^s}{N_c}\big)\bar{\varepsilon}_c$ term (representing average electronic energy of the cation reference phase), (2) $b \times CBM$, (3) $c \times \langle\varepsilon_c^s\rangle$ to substitute $\frac{N_c^s}{N_c}\varepsilon_c^s$, where $\langle\varepsilon_c^s\rangle$ is calculated using computed DOS, (4) and using $d \times \Delta H_f$ as representative of the nuclear repulsive term $\frac{1}{N_c}(\bar{V}_c - V_\alpha)$, and adding an additional fitting parameter e to account for the unknown within the proxies. Eq.(2) now modifies to:

$$\delta\varepsilon_F^{(V_c)} = a^{(V_c)} \times W_c - b^{(V_c)} \times CBM - c^{(V_c)} \times \bar{\varepsilon}_c^s + d^{(V_c)} \times \Delta H_f + e^{(V_c)}, \tag{3}$$

where $\{a^{(V_c)}, b^{(V_c)}, c^{(V_c)}, d^{(V_c)}, e^{(V_c)}\}$ are the free parameters of the model (fitting constants) for the n-type dopability metric, when cation vacancy is the lowest energy (killer) intrinsic acceptor defect.

Anion vacancy

Deriving a more generic description for the anion vacancy formation energy, than that derived in the main text Eq. (6), based on the compound stoichiometry C_xA_y such that $xN_c + yN_a = yn_a$, where N = electrons and n = states.

$$\Delta E_{V_a} = \frac{x}{y}N_c(\varepsilon_F - \bar{\varepsilon}_{VB}) + N_a(\bar{\varepsilon}_a - \bar{\varepsilon}_{VB}) + (\bar{V}_a - V_\alpha) + \Delta\mu_a, \tag{4}$$

p-type dopability metric based on the anion vacancy is then given as:

$$\delta\varepsilon_F^{(V_a)} = \frac{N_a}{\frac{x}{y}N_c}\bar{\varepsilon}_a + VBM - \big(1 + \frac{N_a}{\frac{x}{y}N_c}\big)\bar{\varepsilon}_{VB} + \frac{1}{\frac{x}{y}N_c}(\bar{V}_a - V_\alpha) + \frac{1}{\frac{x}{y}N_c}\Delta\mu_a, \tag{5}$$

Assuming anion-rich conditions for p-type doping ($\Delta\mu_a = 0$), changes Eq.(5) to:

$$\delta\varepsilon_F^{(V_a)} = \frac{N_a}{\frac{x}{y}N_c}\bar{\varepsilon}_a + VBM - \big(1 + \frac{N_a}{\frac{x}{y}N_c}\big)\bar{\varepsilon}_{VB} + \frac{1}{\frac{x}{y}N_c}(\bar{V}_a - V_\alpha), \tag{6}$$

Similar to the n-type dopability metric, using proxies in the p-type dopability metric. (1) $a \times W_a$ (work function of anion reference phase or in case of molecules the first ionization energy) for $\bar{\varepsilon}_a$, (2) $b \times VBM$, (3) average energy (center of mass) of the valence band $c \times \bar{\varepsilon}_{VB}$, and (4) $d \times \Delta H_f$ for the nuclear repulsive term $(\bar{V}_a - V_\alpha)$. Eq.(6) now modifies to:

$$\delta\varepsilon_F^{(V_a)} = a^{(V_a)} \times W_a + b^{(V_a)} \times VBM - c^{(V_a)} \times \langle\varepsilon_a^p\rangle + d^{(V_a)} \times \Delta H_f + e^{(V_a)}, \tag{7}$$

where $\{a^{(V_a)}, b^{(V_a)}, c^{(V_a)}, d^{(V_a)}, e^{(V_a)}\}$ are the fitting constants for the p-type dopability metric, when anion vacancy is the lowest energy (killer) intrinsic donor defect.

Cation Interstitial

$$\Delta E_{I_c} = N_c(\varepsilon_F - \bar{\varepsilon}_c) + N_c^s(\bar{\varepsilon}_c^s - \bar{\varepsilon}_c) + (V_\alpha - \bar{V}_c) - \Delta\mu_c \tag{8}$$

$$\delta\varepsilon_F^{(I_c)} = \varepsilon_F - \bar{\varepsilon}_c + \frac{N_c^s}{N_c}\big(\bar{\varepsilon}_c^s - \bar{\varepsilon}_c\big) + \frac{1}{N_c}(V_\alpha - \bar{V}_c) - \frac{1}{N_c}\Delta\mu_c \tag{9}$$

Ignoring the $\Delta\mu_c$ term at the moment, and applying the proxies to rest of the terms in eq. 9. Note that the cation atom likes to donate electrons and hence act like a donor in an ionic material, and will limit the p-type dopability. Therefore, assuming Fermi energy to be located at the VBM.

$$\delta\varepsilon_F^{(I_c)} = -a^{(I_c)} \times W_c + b^{(I_c)} \times VBM + c^{(I_c)} \times \bar{\varepsilon}_c^s + d^{(I_c)} \times \Delta H_f + e^{(I_c)}, \tag{10}$$

where $\{a^{(I_c)}, b^{(I_c)}, c^{(I_c)}, d^{(I_c)}, e^{(I_c)}\}$ are the fitting constants for the p-type dopability metric, when cation interstitial is the lowest energy (killer) intrinsic donor defect.

Anion Interstitial

$$\Delta E_{I_a} = N_a(\bar{\varepsilon}_{VB} - \bar{\varepsilon}_a) + \frac{x}{y} N_c(\bar{\varepsilon}_{VB} - \varepsilon_F) + (V_\alpha - \bar{V}_a) - \Delta\mu_a \tag{11}$$

$$\delta\varepsilon_F^{(I_a)} = -\frac{N_a}{\frac{x}{y}N_c}\bar{\varepsilon}_a - \varepsilon_F + \big(1 + \frac{N_a}{\frac{x}{y}N_c}\big)\bar{\varepsilon}_{VB} + \frac{1}{\frac{x}{y}N_c}(V_\alpha - \bar{V}_a) - \frac{1}{\frac{x}{y}N_c}\Delta\mu_a \tag{12}$$

Note that the anion atom likes to accept electrons and hence act like an acceptor, and will limit the n-type dopability. Therefore, assuming Fermi energy to be located at the CBM and applying proxies to rest of the terms in eq. 12:

$$\delta\varepsilon_F^{(I_a)} = -a^{(I_a)} \times W_a - b^{(I_a)} \times CBM + c^{(I_a)} \times \bar{\varepsilon}_{VB} + d^{(I_a)} \times \Delta H_f + e^{(I_a)}, \tag{13}$$

where $\{a^{(I_a)}, b^{(I_a)}, c^{(I_a)}, d^{(I_a)}, e^{(I_a)}\}$ are the fitting constants for the n-type dopability metric, when anion interstitial is the lowest energy (killer) intrinsic acceptor defect.

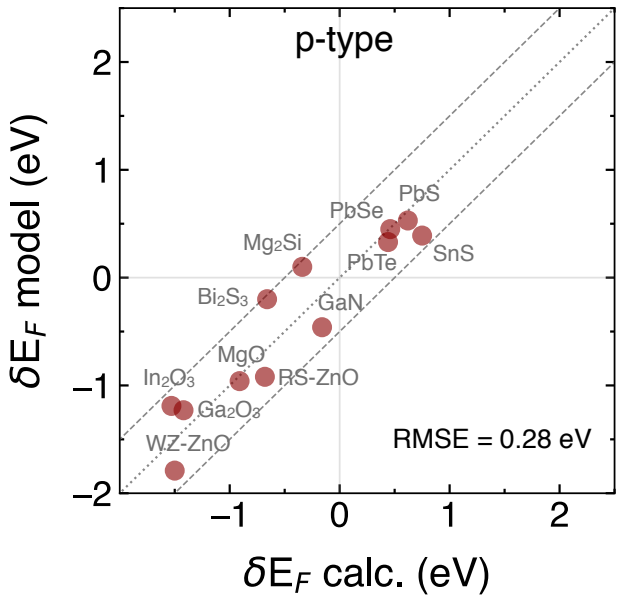

Figure S1: Comparison of the analytic model and the calculated (from first-principles defect calculations) p-type dopability metric $\delta\varepsilon_F^{(p)}$ in case of cation interstitials. The model parameters for Eq.(10) are obtained via linear regression to the calculated values. The expression for the p-type dopability metric based on cation interstitials is given as: $\delta\varepsilon_F^{(p)} = -1.41\,W_c + 0.55\,VBM + 0.01\,\bar{\varepsilon}_c^s - 0.09\,\Delta H_f - 3.14$.

Table S1: Experimental data of the band gap and maximal reported charge carrier concentrations for various binary and ternary semiconductors.

Compound	Band gap (eV)	Carrier concentration (cm^{-3})		References
		n	p	
KAlSb4	0.20	1.00E+19	-	1
$AgFeSe_2$	0.23	5.00E+19	-	2
HfNiSn	0.45	1.00E+19	-	3
ZrNiSn	0.55	8.00E+19	-	3
TiNiSn	0.60	1.00E+19	-	3
InN	0.70	1.00E+19	-	4
CdO	0.90	1.00E+20	-	5–7
$ZnAs_2$	0.90	8.00E+16	-	8
$ZnSnN_2$	0.94	1.00E+21	-	2,9
$AgInSe_2$	0.96	2.50E+18	-	2
$CdAs_2$	1.00	7.00E+16	-	10
$CdSnP_2$	1.16	8.00E+17	-	2

$AgInS_2$	1.18	3.00E+20	-	2
HfCoSb	1.31	1.00E+18	-	1
TiPtSn	1.31	1.00E+21	-	3
TiCoSb	1.42	1.00E+18	-	1
Bi_2S_3	1.45	2.00E+19	-	11,12
ZrCoSb	1.49	5.00E+19	-	1
$CdIn_2Te_4$	1.50	3.50E+15	-	2
$CdIn_2Se_4$	1.55	1.50E+19	-	2
CdSe	1.85	1.00E+18	-	13,14
Sb_2S_3	1.88	1.00E+18	-	15
$ZnIn_2Se_4$	1.92	8.00E+16	-	2
$AgInO_2$	2.00	3.30E+20	-	16,17
Cd_2SnO_4	2.06	1.00E+19	-	18,19
$CdIn_2S_4$	2.10	1.25E+19	-	2
$CdIn_2O_4$	2.23	1.00E+19	-	20
SiC-3C	2.39	1.00E+19	-	21,22
AlP	2.50	1.00E+19	-	23
CdS	2.56	1.00E+21	-	2,24
In_2O_3	2.90	3.00E+20	-	25,26
$ZnGeN_2$	2.90	1.00E+19	-	9
TiO_2	3.03	1.00E+20	-	27,28
$BaSnO_3$	3.10	1.00E+19	-	29
$SrTiO_3$	3.25	1.00E+17	-	30,31
Zn_2SnO_4	3.35	1.00E+19	-	32
$MgIn_2O_4$	3.40	1.00E+19	-	33,34
ZnO	3.43	1.10E+21	-	35
SnO_2	3.60	1.00E+20	-	36,37
ZnS	3.84	1.00E+18	-	14
$SrSnO_3$	3.93	1.00E+19	-	38,39
Ga_2O_3	4.90	1.00E+20	-	40,41
Bi_2Te_3	0.13	1.00E+18	1.00E+19	42
Bi_2Se_3	0.16	1.00E+19	1.00E+19	43–45
InSb	0.17	1.00E+19	1.00E+20	46
$CoSb_3$	0.22	1.00E+21	1.00E+19	1
PbSe	0.27	2.00E+19	1.00E+19	47

InAs	0.30	1.00E+21	1.00E+20	46
$CdSnAs_2$	0.30	5.00E+18	5.00E+18	2
PbTe	0.31	1.00E+20	1.00E+19	48,49
$KGaSb_4$	0.39	2.50E+19	5.00E+18	1
PbS	0.40	4.00E+19	8.00E+18	50
Mg_3Sb_2	0.42	1.00E+19	1.00E+20	51–53
$CoSb_3$	0.50	1.00E+20	1.00E+18	1
$CuFeS_2$	0.53	3.00E+21	7.00E+20	2,54
$CdGeAs_2$	0.53	4.00E+18	2.00E+17	2
Cu_2SnSe_3	0.66	1.00E+18	2.90E+21	2
SnO	0.70	1.00E+17	1.00E+19	55**?**
GaSb	0.73	1.00E+17	1.00E+18	46,56,57
Mg_2Si	0.80	1.00E+20	5.00E+17	58,59
$CuInSe_2$	0.86	7.00E+18	1.00E+19	2
$CuInTe_2$	0.88	2.00E+17	7.50E+19	2
SnSe	0.90	2.00E+19	2.00E+18	60,61
ScN	0.90	1.00E+21	1.00E+20	62–64
Cu_3N	1.00	1.00E+17	1.00E+16	65
SnS	1.10	4.00E+15	1.00E+18	66,67
$CuInS_2$	1.20	1.00E+18	2.00E+19	2
InP	1.34	1.00E+17	1.00E+19	46,68
GaAs	1.42	1.00E+18	5.00E+19	69,70
$CuInO_2$	1.44	1.00E+17	1.00E+17	17,71
CdTe	1.58	2.00E+18	1.00E+16	72–75
$MgGeAs_2$	1.60	3.00E+18	2.00E+19	2
$CdGeP_2$	1.80	1.00E+20	2.00E+18	2
$ZnSiP_2$	2.07	4.80E+18	5.00E+17	2
AlAs	2.10	1.00E+17	1.00E+19	76
GaP	2.30	1.00E+19	1.00E+18	77
ZnSe	2.80	1.00E+19	1.00E+17	78,79
GaN	3.47	5.00E+20	5.00E+17	80
Ag_2SnTe_3	0.08	-	1.00E+20	2
$CuFeTe_2$	0.10	-	5.00E+21	2
$CuFeSe_2$	0.16	-	2.00E+20	2
SnTe	0.18	-	1.00E+21	81

Ag_2GeTe_3	0.25	-	8.00E+17	2
Sb_2Te_3	0.30	-	1.00E+19	82
Cd_4Sb_3	0.30	-	3.00E+19	1,83
Cu_2SnSe_3	0.31	-	3.20E+20	2
$ZnSnSb_2$	0.40	-	1.00E+21	2
Cu_2SnSe_4	0.50	-	1.00E+21	2
Cu_2SnTe_3	0.50	-	1.00E+21	2
CdSb	0.50	-	1.00E+18	84
ZnSb	0.50	-	8.00E+18	85
$AgAlTe_2$	0.56	-	1.00E+17	2,54
Cu_3SbS_4	0.74	-	1.00E+21	2,54
$ZnSnAs_2$	0.74	-	1.00E+21	2,9
Ag_2SnSe_3	0.81	-	1.00E+18	2
Cu_2GeTe_3	0.81	-	3.00E+21	2
$CuGaTe_2$	0.82	-	1.10E+20	2
Cu_3AsSe_4	0.88	-	2.70E+18	2
Cu_2SnS_3	0.91	-	2.50E+21	2
Ag_2GeSe_3	0.91	-	2.00E+17	2
Cu_2GeSe_3	0.94	-	1.40E+21	2
$CuGaSe_2$	0.96	-	1.20E+19	2
NiO	1.00	-	1.00E+19	86–88
$AgGaSe_2$	1.10	-	6.60E+16	2,54
$Cu_2In_4Te_7$	1.10	-	5.30E+18	2
$ZnGeAs_2$	1.16	-	1.00E+15	9
Sb_2Se_3	1.20	-	1.00E+15	89,90
$AgGaTe_2$	1.32	-	1.00E+17	2,54
Cu_3PSe_4	1.40	-	6.00E+17	2
$ZnSnP_2$	1.45	-	1.00E+17	2,9
Cu_2GeS_3	1.50	-	3.00E+17	2
$CdSiAs_2$	1.51	-	1.00E+17	9
AlSb	1.70	-	1.00E+19	2
$ZnGeP_2$	1.80	-	1.00E+17	9,91
$ZnSiAs_2$	2.10	-	1.00E+17	2,9
Cu2O	2.20	-	1.00E+15	28,92–94
LaCuOTe	2.20	-	1.30E+17	95

ZnTe	2.25	-	1.00E+18	96
Cu_3PS_4	2.38	-	1.80E+17	2
$CuGaS_2$	2.38	-	5.40E+17	2
$CuAlS_2$	2.50	-	1.00E+19	2
$CuGaO_2$	2.60	-	1.70E+18	17
$CuAlSe_2$	2.67	-	1.00E+18	2
LaCuOSe	2.80	-	1.00E+20	95,97
$ZnIn_2S_4$	2.90	-	1.00E+17	2
CuI	2.95	-	1.00E+20	2,98,99
$CuAlO_2$	2.97	-	1.30E+17	100,101
LaCuOS	3.10	-	1.00E+19	95,97
$SrCu_2O_2$	3.30	-	1.00E+17	102,103

Table S2: Linear regression fit for n-type dopability metric. $\delta\varepsilon_F^{(n)} = a^{(n)} \times W_c - b^{(n)} \times CBM - c^{(n)} \times \bar{\varepsilon}_c^s + d^{(n)} \times \Delta H_f + e^{(n)}$. Calc. stands for the metric value calculated from defect calculations and Model stands for the metric value calculated from the model following the fit. The corresponding value of the coefficients, along with the error (root mean square error RMSE, and mean absolute error MAE) in the fit are also given. Columns with $\{a\}$, $\{b\}$, ... stands for the model with respective fitting coefficients put to zero. For example $\{a\}$ stands for $a = 0$, such that model does not consist of W_c term. Similarly, $\{a, c, d\}$ stands for $a = c = d = 0$, such that the model now only consists of the CBM and the intercept term, $\delta\varepsilon_F^{(n)} = -b^{(n)} \times CBM + e^{(n)}$.

Compound	Calc.	Model	$\{a\}$	$\{b\}$	$\{c\}$	$\{d\}$	$\{e\}$	$\{a,b\}$	$\{b,c\}$	$\{a,c\}$	$\{c,d\}$	$\{d,e\}$	$\{a,b,c\}$	$\{b,c,d\}$	$\{c,d,e\}$	$\{a,c,d\}$
Bi_2S_3	0.52	0.43	0.35	0.43	0.63	0.43	0.35	0.44	0.83	0.90	0.72	0.35	0.94	0.70	1.05	1.08
Bi_2Se_3	1.12	0.89	0.73	0.42	1.12	0.91	0.77	0.43	0.82	1.26	1.18	0.78	0.94	0.70	1.40	1.37
CdO	2.04	1.74	1.90	1.37	1.51	1.73	1.89	1.34	0.83	1.34	1.46	1.87	0.85	0.85	1.29	1.24
GaN	1.24	0.89	1.57	1.69	0.37	0.83	1.44	1.61	0.73	0.80	0.41	1.33	0.90	0.69	0.82	0.90
Ga_2O_3	0.61	0.79	1.18	0.61	0.66	0.83	1.24	0.55	0.30	1.31	0.41	1.34	0.70	0.69	0.83	0.90
In_2O_3	1.65	1.91	1.89	0.81	1.89	1.96	1.99	0.78	0.60	1.78	1.68	2.09	0.74	0.84	1.47	1.39
MgO	-1.42	-1.43	-1.38	0.35	-1.35	-1.42	-1.49	0.40	0.82	-0.98	-1.41	-1.45	0.67	1.12	-1.47	-1.07
Mg_2Si	0.79	1.30	1.27	1.92	1.02	1.23	1.09	1.94	1.43	0.24	1.23	0.94	0.96	1.12	0.54	0.56
PbS	0.47	0.49	0.52	0.69	0.55	0.47	0.49	0.69	0.85	0.79	0.63	0.46	0.93	0.74	0.90	0.95
PbSe	0.64	0.63	0.62	0.66	0.72	0.62	0.60	0.66	0.85	0.91	0.79	0.59	0.93	0.74	1.02	1.05
PbTe	0.63	0.74	0.70	0.68	0.85	0.74	0.68	0.69	0.88	0.97	0.93	0.66	0.94	0.74	1.13	1.14
ScN	2.16	1.70	1.18	1.13	1.82	1.72	1.18	1.18	1.27	0.78	1.81	1.19	0.82	1.23	0.76	0.72
SnO	0.20	0.16	0.29	0.19	0.31	0.19	0.33	0.17	0.50	1.00	0.25	0.39	0.83	0.62	0.84	0.93
SnS	-0.10	0.19	0.39	0.56	0.22	0.17	0.36	0.55	0.69	0.80	0.28	0.34	0.92	0.62	0.87	0.95
Rocksalt-ZnO	1.44	1.24	0.94	1.11	1.26	1.24	0.91	1.15	1.14	0.59	1.26	0.91	0.81	1.14	0.52	0.54
Wurtzite-ZnO	1.68	1.99	1.53	1.05	2.10	2.02	1.57	1.09	1.12	1.19	2.03	1.61	0.80	1.14	1.11	1.02
Coefficients																
a		1.40	0.00	-0.15	2.02	1.45	0.10	0.00	0.87	0.00	2.08	0.16	0.00	0.66	0.20	0.00
b		0.60	0.48	0.00	0.64	0.61	0.53	0.00	0.00	0.45	0.61	0.55	0.00	0.00	0.46	0.38
c		-0.05	-0.11	-0.11	0.00	-0.05	-0.10	-0.10	0.00	0.00	0.00	-0.09	0.00	0.00	0.00	0.00
d		0.03	0.10	0.27	-0.07	0.00	0.05	0.26	0.10	-0.12	0.00	0.00	0.05	0.00	0.00	0.00
e		4.79	-0.02	1.45	6.59	4.85	0.00	2.04	4.66	-1.06	7.15	0.00	0.98	3.53	0.00	-0.48
RMSE		0.26	0.39	0.72	0.32	0.26	0.38	0.72	0.82	0.64	0.34	0.38	0.86	0.84	0.63	0.67
MAE		0.21	0.29	0.54	0.24	0.21	0.28	0.54	0.64	0.55	0.27	0.27	0.68	0.59	0.53	0.58
R^2		0.91	0.80	0.30	0.86	0.91	0.81	0.30	0.10	0.46	0.84	0.80	0.01	0.06	0.47	0.41

Table S3: Linear regression fit for p-type dopability metric. $\delta\varepsilon_F^{(p)} = a^{(p)} \times W_a + b^{(p)} \times VBM - c^{(p)} \times \bar{\varepsilon}_{VB} + d^{(p)} \times \Delta H_f + e^{(p)}$. Calc. stands for the metric value calculated from defect calculations and Model stands for the metric value calculated from the model following the fit. The corresponding value of the coefficients, along with the error (root mean square error RMSE, and mean absolute error MAE) in the fit are also given. Columns with $\{a\}$, $\{b\}$, ... stands for the model with respective fitting coefficients put to zero. For example $\{a\}$ stands for $a = 0$, such that model does not consist of W_c term. Similarly, $\{a, c, d\}$ stands for $a = c = d = 0$, such that the model now only consists of the VBM and the intercept term, $\delta\varepsilon_F^{(p)} = b^{(p)} \times VBM + e^{(p)}$.

Compound	Calc.	Model	$\{a\}$	$\{b\}$	$\{c\}$	$\{d\}$	$\{e\}$	$\{a,b\}$	$\{b,c\}$	$\{a,c\}$	$\{c,d\}$	$\{d,e\}$	$\{a,b,c\}$	$\{b,c,d\}$	$\{c,d,e\}$	$\{a,c,d\}$
Bi_2S_3	-0.51	-0.20	-0.06	-0.19	0.03	-0.02	0.23	-0.04	0.29	0.01	0.00	-0.15	0.33	0.12	-0.07	0.02
Bi_2Se_3	-0.06	-0.09	0.02	-0.08	0.11	0.06	0.21	0.01	0.30	0.11	0.08	-0.14	0.32	0.17	-0.17	0.11
CdO	0.19	0.29	0.24	0.28	0.09	0.23	0.01	0.37	-0.09	0.05	0.09	0.05	-0.03	-0.13	0.13	0.05
GaN	-0.36	-0.03	-0.03	-0.04	-0.21	0.02	0.00	0.27	0.00	-0.30	-0.25	-0.15	0.14	-0.20	0.02	-0.29
Ga_2O_3	-1.33	-1.00	-1.06	-1.01	-1.05	-1.03	-0.77	-0.93	-0.22	-1.01	-1.04	-0.51	-0.22	-0.13	-0.44	-1.01
In_2O_3	-0.59	-0.83	-0.79	-0.83	-0.73	-0.78	-0.41	-0.70	-0.15	-0.73	-0.74	-0.32	-0.12	-0.13	-0.29	-0.73
MgO	-0.58	-0.50	-0.48	-0.48	-0.33	-0.64	-0.43	-0.75	-0.51	-0.25	-0.25	0.14	-0.63	-0.13	-0.04	-0.27
Mg_2Si	0.25	0.60	0.50	0.60	0.63	0.55	0.06	0.21	0.46	0.74	0.65	-0.13	0.29	0.57	-0.28	0.74
PbS	0.49	0.29	0.45	0.31	0.53	0.42	0.51	0.34	0.22	0.51	0.52	0.19	0.24	0.12	0.09	0.51
PbSe	0.73	0.42	0.45	0.42	0.46	0.46	0.30	0.39	0.24	0.46	0.45	0.06	0.24	0.17	0.01	0.46
PbTe	0.67	0.59	0.30	0.56	0.28	0.43	-0.35	0.20	0.45	0.40	0.29	-0.43	0.29	0.54	-0.43	0.40
ScN	0.61	0.83	0.81	0.82	0.63	0.72	0.37	0.86	-0.19	0.55	0.64	0.45	-0.13	-0.20	0.47	0.54
SnO	0.55	0.45	0.52	0.46	0.47	0.43	0.36	0.49	-0.12	0.41	0.48	0.36	-0.08	-0.13	0.32	0.41
SnS	0.70	0.40	0.35	0.39	0.27	0.39	0.10	0.40	0.21	0.26	0.26	-0.08	0.22	0.12	-0.04	0.26
Rocksalt-ZnO	-0.22	-0.21	-0.09	-0.20	-0.03	-0.17	0.09	-0.15	-0.17	-0.05	-0.02	0.15	-0.15	-0.13	0.07	-0.05
Wurtzite-ZnO	-0.02	-0.48	-0.58	-0.50	-0.64	-0.56	-0.56	-0.45	-0.20	-0.63	-0.64	-0.32	-0.19	-0.13	-0.24	-0.63
Coefficients																
a		0.09	0.00	0.08	-0.03	0.03	-0.16	0.00	0.03	0.00	-0.02	-0.11	0.00	0.08	-0.09	0.00
b		-0.03	0.20	0.00	0.37	0.11	0.50	0.00	0.00	0.36	0.38	0.35	0.00	0.00	0.19	0.35
c		-0.37	-0.18	-0.35	0.00	-0.23	0.23	-0.31	0.00	0.00	0.00	0.12	0.00	0.00	0.00	0.00
d		-0.12	-0.01	-0.11	0.02	0.00	0.21	0.02	0.12	0.00	0.00	0.00	0.17	0.00	0.00	0.00
e		2.81	2.14	2.77	1.84	2.29	0.00	1.89	0.70	2.00	1.90	0.00	0.41	0.92	0.00	2.00
RMSE		0.25	0.28	0.25	0.31	0.27	0.45	0.31	0.51	0.31	0.31	0.51	0.52	0.53	0.52	0.31
MAE		0.22	0.23	0.22	0.25	0.22	0.37	0.26	0.43	0.26	0.25	0.43	0.43	0.44	0.44	0.26
R^2		0.81	0.77	0.81	0.72	0.78	0.40	0.71	0.22	0.71	0.72	0.21	0.20	0.17	0.19	0.71

Table S4: Calculated cation vacancy formation energy ΔH at the conduction band minimum (CBM) and the n-type pinning energy $\varepsilon_F^{(n)}$ relative to the vacuum, along with the charge state q. In the model cation-rich conditions are assumed.

Compound	Defect (D)	Charge (q)	ΔH (D, q) @CBM	$\varepsilon_F^{(n)}$
Bi_2S_3	V_{Bi}	-3	1.55	-3.65
Bi_2Se_3	V_{Bi}	-3	3.05	-3.81
CdO	V_{Cd}	-2	4.08	-2.86
GaN	V_{Ga}	-3	3.73	-2.28
Ga_2O_3	V_{Ga}	-3	1.84	-3.09
In_2O_3	V_{In}	-3	6.35	-3.35
MgO	V_{Mg}	-2	-2.85	-0.54
Mg_2Si	V_{Mg}	-2	1.58	-1.99
PbS	V_{Pb}	-2	0.93	-3.36
PbSe	V_{Pb}	-2	1.27	-3.46
PbTe	V_{Pb}	-2	1.26	-3.77
ScN	V_{Sc}	-3	6.48	-1.04
SnO	V_{Sn}	-2	0.40	-3.57
SnS	V_{Sn}	-2	-0.20	-3.93
Rocksalt ZnO	V_{Zn}	-2	2.87	-1.98
Wurtzite ZnO	V_{Zn}	-2	3.36	-2.68

Table S5: Calculated anion vacancy formation energy ΔH at the valence band maximum (VBM) and the p-type pinning energy $\varepsilon_F^{(p)}$ relative to the vacuum, along with the charge state, q. In the model anion-rich conditions are assumed. For Mg_2Si, the lowest energy intrinsic donor is cation interstitial instead of the anion vacancy.

Compound	Defect (D)	Charge (q)	ΔH (D, q) @VBM	$\varepsilon_F^{(p)}$
Bi_2S_3	V_S	2	-1.02	-5.08
Bi_2Se_3	V_{Se}	2	-0.11	-5.27
CdO	V_O	2	0.37	-5.89
GaN	V_N	3	-1.07	-6.61
Ga_2O_3	V_O	2	-2.66	-7.17
In_2O_3	V_O	2	-1.18	-7.13
MgO	V_O	2	-1.15	-6.72
Mg_2Si	Mg_i	2	-0.67	-3.21
PbS	V_S	2	0.97	-4.70
PbSe	V_{Se}	2	1.45	-5.08
PbTe	V_{Te}	2	1.33	-5.18
ScN	V_N	3	1.84	-4.73
SnO	V_O	2	1.10	-5.05
SnS	V_S	2	1.40	-5.60
Rocksalt ZnO	V_O	2	-0.44	-6.59
Wurtzite ZnO	V_O	2	-0.03	-7.72

Table S6: Reference phase ionization energy (for gas phase) and work function (for solid phase) with respect to the vacuum, obtained from Refs.[54,104] Cohesive energy of a solid or gas (molecule) phase is the energy required to break it into its constituent gas phase, and is obtained from page 50 of Ref.[105]

Reference	Ionization Energy or Work function			Cohesive Energy	
phase	(eV)	Method	Additional Details	(kJ/mol)	in eV/atom
Bi (s)	-4.34	Photoelectric effect	Polycrystalline sample	-210.0	-2.18
Cd (s)	-4.08	Contact potential difference	Polycrystalline sample	-112.0	-1.16
Ga (s)	-4.32	Photoelectric effect	Polycrystalline sample	-271.0	-2.81
In (s)	-4.09	Photoelectric effect	Polycrystalline sample	-243.0	-2.52
Mg (s)	-3.66	Photoelectric effect	Polycrystalline sample	-145.0	-1.51
N_2 (g)	-14.53			-945.0	-4.90
O_2 (g)	-13.62			-498.0	-2.58
Pb (s)	-4.25	Photoelectric effect	Polycrystalline sample	-196.0	-2.03
S (s)	-10.36			-275.0	-2.85
Sb (s)	-4.70	Photoelectric effect	100 plane	-265.0	-2.75
Sc (s)	-3.50	Photoelectric effect	Polycrystalline sample	-376.0	-3.90
Se (s)	-5.90	Photoelectric effect	Polycrystalline sample	-237.0	-2.46
Si (s)	-4.60	Photoelectric effect	111 plane	-446.0	-4.63
Si (s)	-4.91	Contact potential difference	100 plane		
Sn (s)	-4.42	Contact potential difference	Polycrystalline sample	-303.0	-3.14
Te (s)	-4.95	Photoelectric effect	Polycrystalline sample	-211.0	-2.19
Zn (s)	-3.63	Photoelectric effect	Polycrystalline sample	-130.0	-1.35
Zn (s)	-4.90	Contact potential difference	Polycrystalline sample		

Table S7: Intrinsic materials properties of compounds both from experiments and calculated from the respective level of theory. Band gap (E_g), Ionization Energy (IE) or VBM, Electron Affinity (EA) or CBM, Enthalpy of formation[106] (ΔH^f), Bulk Modulus (B), Volume (Ω), Average energy of cation-s ($\bar{\varepsilon}_c^s$) and valence band ($\bar{\varepsilon}_{VB}$) states from the calculated density of states (DOS). IE, EA, $\bar{\varepsilon}_c^s$, $\bar{\varepsilon}_{VB}$ are calculated with respect to vacuum.

Compound	Level of theory	E_g (eV)		IE (eV)		EA (eV)		ΔH^f (eV/unit)	B (GPa)		Ω (Å^3/unit)		DOS	DOS
		Exp.	Calc.	Exp.	Calc.	Exp.	Calc.	Exp.	Exp.	Calc.	Exp.	Calc.	$\bar{\varepsilon}_c^s$	$\bar{\varepsilon}_{VB}$
Bi_2S_3[107,108]	DFT+SOC+GW	1.45	1.42	-5.6	-5.59	-4.15	-4.17	-1.41	39.7	16.9	125.4	123.5	-14.2	-6.15
Bi_2Se_3[109,110]	DFT+SOC+GW	0.16	0.40	-5.5	-5.33	-5.3	-4.93	-1.6	32.9		141.6	144.6	-14.0	-6.0
CdO[7,111]	HSE (α =0.25)	0.84	0.92	-5.7	-5.70	-4.8	-4.59	-2.68	150			26.2		-4.72
GaN[28,112]	HSE (0.27)	3.47	3.48	-6.8	-6.97	-3.33	-3.52	-1.63	187	171.0	22.8	22.6		-5.09
Ga_2O_3[41,113]	DFT+GW	4.80	4.95	-8.5		-3.7		-11.35	150	153.8	52.4	54.8		-8.79
In_2O_3[114,115]	DFT+GW	2.67	2.47	-7.7		-5.0		-9.6	194.2	147.9	67.9	68.1		-8.09
MgO[111,116]	HSE (0.40)	7.80	7.97	-7.15	-7.20	0.65	0.61	-6.26	152	181.6	18.6	18.1		-8.06
Mg_2Si[117]	DFT+GW	0.78	0.78		-3.55		-2.77	-3.26		54.5		64.2		-5.35
PbS[118,119]	HSE+SOC+G_0W_0	0.29	0.39	-4.6	-4.21	-4.31	-3.82	-1.03	62.8	52.8	52.3	52.8	-10.8	-4.9
PbSe[118,120]	HSE+SOC+G_0W_0	0.15	0.26	-4.75	-4.35	-4.6	-4.09	-1.04	54.1	46.6	57.4	58.6	-11.1	-4.73
PbTe[48,118]	HSE+SOC+G_0W_0	0.19	0.19	-4.6	-4.51	-4.41	-4.32	-0.71	39.8	38.5	67.8	69.1	-11.7	-5.38
ScN[64]	HSE (0.25)	0.90	0.91	-4.0	-4.12	-3.1	-3.21	-3.26	182	189.1		22.7		-3.12
SnO[121]	HSE (0.32)	0.70	0.73		-4.50		-3.77	-2.96	48	43.6	69.9	74.6	-11.0	-4.3
SnS[66,122]	DFT+GW	1.08	1.17		-4.90		-3.83	-1.14	36.6		191.9	199.5	-12.1	-4.7
Rocksalt ZnO[123]	HSE (0.30)	3.1	3.07		-6.81		-3.66	-3.39	202.5	192.7	19.5	19.6		-6.33
Wurtzite ZnO[28,35]	HSE (0.375)	3.43	3.43	-7.82	-7.73	-4.39	-4.5	-3.63	142.4	149.1	23.8	23.9		-7.26

References

(1) Gorai, P.; Goyal, A.; Toberer, E. S.; Stevanović, V. A simple chemical guide for finding novel n-type dopable Zintl pnictide thermoelectric materials. Journal of Materials Chemistry A **2019**, 7, 19385–19395.

(2) Miller, S. A.; Dylla, M.; Anand, S.; Gordiz, K.; Snyder, G. J.; Toberer, E. S. Empirical modeling of dopability in diamond-like semiconductors. npj Computational Materials **2018**, 4, 71.

(3) Yu, Y. G.; Zhang, X.; Zunger, A. Natural off-stoichiometry causes carrier doping in half-Heusler filled tetrahedral structures. Physical Review B **2017**, 95, 085201.

(4) Anderson, P. A. Indium Nitride: An Investigation of Growth, Electronic Structure and Doping. Ph.D. thesis, University of Canterbury, 2006.

(5) Sachet, E.; Shelton, C. T.; Harris, J. S.; Gaddy, B. E.; Irving, D. L.; Curtarolo, S.; Donovan, B. F.; Hopkins, P. E.; Sharma, P. A.; Sharma, A. L.; Ihlefeld, J.; Franzen, S.; Maria, J.-P. Dysprosium-doped cadmium oxide as a gateway material for mid-infrared plasmonics. Nature Materials **2015**, 14, 414–420.

(6) Dou, Y.; Egdell, R.; Walker, T.; Law, D.; Beamson, G. N-type doping in CdO ceramics: a study by EELS and photoemission spectroscopy. Surface Science **1998**, 398, 241–258.

(7) Burbano, M.; Scanlon, D. O.; Watson, G. W. Sources of Conductivity and Doping Limits in CdO from Hybrid Density Functional Theory. Journal of the American Chemical Society **2011**, 133, 15065–15072.

(8) Zinc arsenide (ZnAs2) resistivity, carrier concentration and mobility, thermoelectric power and thermal conductivity: Datasheet from Landolt-Börnstein - Group

III Condensed Matter · Volume 41C: "Non-Tetrahedrally Bonded Elements and Binary Compounds I" in. https://materials.springer.com/lb/docs/sm{_}lbs{_}978-3-540-31360-1{_}296.

(9) Martinez, A. D.; Fioretti, A. N.; Toberer, E. S.; Tamboli, A. C. Synthesis, structure, and optoelectronic properties of II–IV–V 2 materials. Journal of Materials Chemistry A **2017**, 5, 11418–11435.

(10) CdAs2 rt charge carrier concentration: Datasheet from "PAULING FILE Multinaries Edition – 2012" in SpringerMaterials. https://materials.springer.com/isp/physical-property/docs/ppp{_}2798f764b55658e860c4c62408f637f9.

(11) Biswas, K.; Zhao, L.-D.; Kanatzidis, M. G. Tellurium-Free Thermoelectric: The Anisotropic n-Type Semiconductor Bi2S3. Advanced Energy Materials **2012**, 2, 634–638.

(12) Bi2S3 charge carrier concentration: Datasheet from "PAULING FILE Multinaries Edition – 2012" in Spr ingerMaterials. https://materials.springer.com/isp/physical-property/docs/ppp{_}4c819d3b38b28edc32d590df4441cd18.

(13) Yu, D. n-Type Conducting CdSe Nanocrystal Solids. Science **2003**, 300, 1277–1280.

(14) Sze, S.; Ng, K. K. Physics of Semiconductor Devices; John Wiley & Sons, Inc.: Hoboken, NJ, USA, 2006.

(15) Sb2S3 energy gap: Datasheet from "PAULING FILE Multinaries Edition – 2012" in SpringerMaterials. https://materials.springer.com/isp/physical-property/docs/ppp{_}2ecbfb3a11855a7587d8051fc68d778f.

(16) Ibuki, S.; Yanagi, H.; Ueda, K.; Kawazoe, H.; Hosono, H. Preparation of n -type conductive transparent thin films of AgInO2:Sn with delafossite-type structure by pulsed laser deposition. Journal of Applied Physics **2000**, 88, 3067–3069.

(17) Kumar, M.; Zhao, H.; Persson, C. Study of band-structure, optical properties and native defects in A I B III O 2 (A I = Cu or Ag, B III = Al, Ga or In) delafossites. Semiconductor Science and Technology **2013**, 28, 065003.

(18) Kumaravel, R.; Ramamurthi, K. Structural, optical and electrical properties of In-doped Cd2SnO4 thin films by spray pyrolysis method. Journal of Alloys and Compounds **2011**, 509, 4390–4393.

(19) Cd2SnO4 rt charge carrier concentration: Datasheet from "PAULING FILE Multinaries Edition – 2012" in SpringerMaterials. `https://materials.springer.com/isp/physical-property/docs/ppp{\_}0e21621053d5c7fa81f5fce26ac674f7`.

(20) Segev, D.; Wei, S.-H. Structure-derived electronic and optical properties of transparent conducting oxides. Physical Review B **2005**, 71, 125129.

(21) Colston, G.; Myronov, M. Electrical properties of n-type 3C-SiC epilayers in situ doped with extremely high levels of phosphorus. Semiconductor Science and Technology **2018**, 33, 114007.

(22) SiC 3C charge carrier concentration: Datasheet from "PAULING FILE Multinaries Edition – 2012" in Sp ringerMaterials. `https://materials.springer.com/isp/physical-property/docs/ppp{\_}e369e6c5cbdc9d2f3f703e5c77ae2652`.

(23) Aluminum phosphide (AlP), electrical and thermal transport: Datasheet from Landolt-Börnstein - Group III Condensed Matter Volume 41A1: "Group IV Elements, IV-IV and III-V Compounds. Part b - Electronic, Transport, Optical and Other Properties" in Sprin. `https://materials.springer.com/lb/docs/sm{\_}lbs{\_}978-3-540-31356-4{\_}67`.

(24) Crandall, R. S. Electrical Conduction in n-Type Cadmium Sulfide at Low Temperatures. Physical Review **1968**, 169, 577–584.

(25) Limpijumnong, S.; Reunchan, P.; Janotti, A.; Van De Walle, C. G. Hydrogen doping in indium oxide: An ab initio study. Physical Review B - Condensed Matter and Materials Physics **2009**, 80, 1–4.

(26) Walsh, A.; Da Silva, J. L. F.; Wei, S.-H.; Körber, C.; Klein, A.; Piper, L. F. J.; DeMasi, A.; Smith, K. E.; Panaccione, G.; Torelli, P.; Payne, D. J.; Bourlange, A.; Egdell, R. G. Physical Review Letters **2008**, 100, 167402.

(27) Bally, A. Electronic properties of nano-crystalline titanium dioxide thin films. Ph.D. thesis, 1999.

(28) Stevanović, V.; Lany, S.; Ginley, D. S.; Tumas, W.; Zunger, A. Assessing capability of semiconductors to split water using ionization potentials and electron affinities only. Physical chemistry chemical physics : PCCP **2014**, 16, 3706–14.

(29) Kim, H. J.; Kim, U.; Kim, T. H.; Kim, J.; Kim, H. M.; Jeon, B.-G.; Lee, W.-J.; Mun, H. S.; Hong, K. T.; Yu, J.; Char, K.; Kim, K. H. Physical Review B **2012**, 86, 165205.

(30) Tufte, O. N.; Chapman, P. W. Electron Mobility in Semiconducting Strontium Titanate. Physical Review **1967**, 155, 796–802.

(31) van Benthem, K.; Elsässer, C.; French, R. H. Bulk electronic structure of SrTiO3: Experiment and theory. Journal of Applied Physics **2001**, 90, 6156–6164.

(32) Dimitrievska, M.; Ivetić, T. B.; Litvinchuk, A. P.; Fairbrother, A.; Miljević, B. B.; Štrbac, G. R.; Pérez Rodríguez, A.; Lukić-Petrović, S. R. Eu 3+ -Doped Wide Band Gap Zn 2 SnO 4 Semiconductor Nanoparticles: Structure and Luminescence. The Journal of Physical Chemistry C **2016**, 120, 18887–18894.

(33) Kawazoe, H.; Ueda, K. Transparent Conducting Oxides Based on the Spinel Structure. Journal of the American Ceramic Society **2004**, 82, 3330–3336.

(34) Ueda, N.; Omata, T.; Hikuma, N.; Ueda, K.; Mizoguchi, H.; Hashimoto, T.; Kawazoe, H. New oxide phase with wide band gap and high electroconductivity, MgIn 2 O 4. Applied Physics Letters **1992**, 61, 1954–1955.

(35) Özgür, Ü.; Alivov, Y. I.; Liu, C.; Teke, A.; Reshchikov, M. A.; Doğan, S.; Avrutin, V.; Cho, S.-J.; Morkoç, H. A comprehensive review of ZnO materials and devices. Journal of Applied Physics **2005**, 98, 1–103.

(36) Edwards, P. P.; Porch, A.; Jones, M. O.; Morgan, D. V.; Perks, R. M. Basic materials physics of transparent conducting oxides. Dalton Transactions **2004**, 2995.

(37) Nagasawa, M.; Shionoya, S. Exciton structure in optical absorption of SnO2 crystals. Physics Letters **1966**, 22, 409–410.

(38) Hadjarab, B.; Bouguelia, A.; Trari, M. Synthesis, physical and photo electrochemical characterization of La-doped SrSnO3. Journal of Physics and Chemistry of Solids **2007**, 68, 1491–1499.

(39) Bellal, B.; Hadjarab, B.; Bouguelia, A.; Trari, M. Visible light photocatalytic reduction of water using SrSnO3 sensitized by CuFeO2. Theoretical and Experimental Chemistry **2009**, 45, 172–179.

(40) Lany, S. Defect phase diagram for doping of Ga2O3. APL Materials **2018**, 6.

(41) Pearton, S. J.; Yang, J.; Cary, P. H.; Ren, F.; Kim, J.; Tadjer, M. J.; Mastro, M. A. A review of Ga 2 O 3 materials, processing, and devices. Applied Physics Reviews **2018**, 5, 011301.

(42) Yashima, I.; Watanave, H.; Ogisu, T.; Tsukuda, R.; Sa̋to, S. Thermoelectric Properties and Hall Effect of Bi 2 Te 3 - x Se x Polycrystalline Materials Prepared by a Hot Press Method. Japanese Journal of Applied Physics **1998**, 37, 2472–2473.

(43) Hor, Y. S.; Richardella, A.; Roushan, P.; Xia, Y.; Checkelsky, J. G.; Yazdani, A.; Hasan, M. Z.; Ong, N. P.; Cava, R. J. Physical Review B **2009**, 79, 195208.

(44) Li, M.; Wang, Z.; Yang, L.; Li, D.; Yao, Q. R.; Rao, G. H.; Gao, X. P. A.; Zhang, Z. Physical Review B **2017**, 96, 075152.

(45) Filip, M. R.; Patrick, C. E.; Giustino, F. Physical Review B **2013**, 87, 205125.

(46) Levinshtein, M.; Rumyantsev, S. L.; Shur, M. Handbook series on semiconductor parameters. Vol. 1, Si, Ge, C (diamond), GaAs, GaP, GaSb, InA Singapore ; New Jersey : World Scientific, 1996.

(47) PbSe charge carrier concentration: Datasheet from "PAULING FILE Multinaries Edition – 2012" in Spri ngerMaterials. `https://materials.springer.com/isp/physical-property/docs/ppp{\_}7ec1c948a29528b9acf9cb40911ea701`.

(48) Goyal, A.; Gorai, P.; Toberer, E. S.; Stevanović, V. First-principles calculation of intrinsic defect chemistry and self-doping in PbTe. npj Computational Materials **2017**, 3, 42.

(49) Male, J.; Agne, M. T.; Goyal, A.; Anand, S.; Witting, I. T.; Stevanović, V.; Snyder, G. J. The importance of phase equilibrium for doping efficiency: iodine doped PbTe. Materials Horizons **2019**,

(50) PbS charge carrier concentration: Datasheet from "PAULING FILE Multinaries Edition – 2012" in Sp ringerMaterials. `https://materials.springer.com/isp/physical-property/docs/ppp{\_}45dbe0d0b9aad1149f9773f6b8ef8316`.

(51) Ohno, S.; Imasato, K.; Anand, S.; Tamaki, H.; Kang, S. D.; Gorai, P.; Sato, H. K.; Toberer, E. S.; Kanno, T.; Snyder, G. J. Phase Boundary Mapping to Obtain n-type Mg3Sb2-Based Thermoelectrics. Joule **2018**, 2, 141–154.

(52) Shuai, J.; Wang, Y.; Kim, H. S.; Liu, Z.; Sun, J.; Chen, S.; Sui, J.; Ren, Z. Thermoelectric properties of Na-doped Zintl compound: Mg3NaSb2. Acta Materialia **2015**, 93, 187–193.

(53) Zhang, J.; Song, L.; Pedersen, S. H.; Yin, H.; Hung, L. T.; Iversen, B. B. Discovery of high-performance low-cost n-type Mg3Sb2-based thermoelectric materials with multi-valley conduction bands. Nature Communications **2017**, 8, 13901.

(54) Lide R., D., Ed. CRC Handbook of Chemistry and Physics, 9th ed.; 2009; pp 12–114.

(55) Hosono, H.; Ogo, Y.; Yanagi, H.; Kamiya, T. Bipolar Conduction in SnO Thin Films. Electrochemical and Solid-State Letters **2011**, 14, H13.

(56) Strauss, A. J. Physical Review **1961**, 121, 1087–1090.

(57) Mitchel, W. C.; Elhamri, S.; Haugan, H. J.; Berney, R.; Mou, S.; Brown, G. J. Electrical properties of n-type GaSb substrates and p-type GaSb buffer layers for InAs/InGaSb superlattice infrared detectors. AIP Advances **2015**, 5, 097219.

(58) Nolas, G. S.; Wang, D.; Beekman, M. Transport properties of polycrystalline Mg2Si1-ySby. Physical Review B **2007**, 76, 235204.

(59) Kolezynski, A.; Nieroda, P.; Wojciechowski, K. T. Li doped Mg2Si p-type thermoelectric material: Theoretical and experimental study. Computational Materials Science **2015**, 100, 84–88.

(60) SnSe rt charge carrier concentration: Datasheet from "PAULING FILE Multinaries Edition – 2012" i n SpringerMaterials. `https://materials.springer.com/isp/physical-property/docs/ppp{\_}524046fdf85db860ef88122fcba273a8`.

(61) Duong, A. T.; Nguyen, V. Q.; Duvjir, G.; Duong, V. T.; Kwon, S.; Song, J. Y.; Lee, J. K.; Lee, J. E.; Park, S.; Min, T.; Lee, J.; Kim, J.; Cho, S. Achieving ZT=2.2 with Bi-doped n-type SnSe single crystals. Nature Communications **2016**, 7, 13713.

(62) Deng, R.; Ozsdolay, B. D.; Zheng, P. Y.; Khare, S. V.; Gall, D. Optical and transport measurement and first-principles determination of the ScN band gap. Physical Review B **2015**, 91, 045104.

(63) Saha, B.; Garbrecht, M.; Perez-Taborda, J. A.; Fawey, M. H.; Koh, Y. R.; Shakouri, A.; Martin-Gonzalez, M.; Hultman, L.; Sands, T. D. Compensation of native donor doping in ScN: Carrier concentration control and p -type ScN. Applied Physics Letters **2017**, 110, 252104.

(64) Kumagai, Y.; Tsunoda, N.; Oba, F. Point Defects and p-Type Doping in ScN from First Principles. Physical Review Applied **2018**, 9, 34019.

(65) Fioretti, A. N.; Schwartz, C. P.; Vinson, J.; Nordlund, D.; Prendergast, D.; Tamboli, A. C.; Caskey, C. M.; Tuomisto, F.; Linez, F.; Christensen, S. T.; Toberer, E. S.; Lany, S.; Zakutayev, A. Understanding and control of bipolar self-doping in copper nitride. Journal of Applied Physics **2016**, 119, 181508.

(66) Vidal, J.; Lany, S.; D'Avezac, M.; Zunger, A.; Zakutayev, A.; Francis, J.; Tate, J. Band-structure, optical properties, and defect physics of the photovoltaic semiconductor SnS. Applied Physics Letters **2012**, 100.

(67) Xiao, Z.; Ran, F.-Y.; Hosono, H.; Kamiya, T. Route to n -type doping in SnS. Applied Physics Letters **2015**, 106, 152103.

(68) Bugajski, M.; Lewandowski, W. Concentration-dependent absorption and photoluminescence of n -type InP. Journal of Applied Physics **1985**, 57, 521–530.

(69) Neave, J. H.; Dobson, P. J.; Harris, J. J.; Dawson, P.; Joyce, B. A. Silicon doping of MBE-grown GaAs films. Applied Physics A Solids and Surfaces **1983**, 32, 195–200.

(70) Sun, S.; Armour, E.; Zheng, K.; Schaus, C. Zinc and tellurium doping in GaAs and AlGaAs grown by MOCVD. Journal of Crystal Growth **1991**, 113, 103–112.

(71) Yanagi, H.; Hase, T.; Ibuki, S.; Ueda, K.; Hosono, H. Bipolarity in electrical conduction of transparent oxide semiconductor CuInO2 with delafossite structure. Applied Physics Letters **2001**, 78, 1583–1585.

(72) Segall, B.; Lorenz, M. R.; Halsted, R. E. Physical Review **1963**, 129, 2471–2481.

(73) Perrenoud, J.; Kranz, L.; Gretener, C.; Pianezzi, F.; Nishiwaki, S.; Buecheler, S.; Tiwari, A. N. A comprehensive picture of Cu doping in CdTe solar cells. Journal of Applied Physics **2013**, 114, 174505.

(74) Nagaoka, A.; Kuciauskas, D.; McCoy, J.; Scarpulla, M. A. High p-type doping, mobility, and photocarrier lifetime in arsenic-doped CdTe single crystals. Applied Physics Letters **2018**, 112, 192101.

(75) Su, C. H. Energy band gap, intrinsic carrier concentration, and Fermi level of CdTe bulk crystal between 304 and 1067 K. Journal of Applied Physics **2008**, 103.

(76) Aluminum arsenide (AlAs), electrical and thermal conductivity, carrier concentration: Datasheet from Landolt-Börnstein - Group III Condensed Matter Volume 41A1: "Group IV Elements, IV-IV and III-V Compounds. Part b - Electronic, Transport, Optical an. `https://materials.springer.com/lb/docs/sm{\_}lbs{\_}978-3-540-31356-4{\_}84`.

(77) GaP rt charge carrier concentration: Datasheet from "PAULING FILE Multinaries Edition – 2012" in SpringerMaterials. `https://materials.springer.com/isp/physical-property/docs/ppp{\_}5215e83ea64ca9960e3ef91c61d54fb3`.

(78) Simpson, J.; Wallace, J. M.; Wang, S. Y.; Stewart, H.; Hunter, J. J.; Adams, S. J.; Prior, K. A.; Cavenett, B. C. N-type doping of molecular beam epitaxial zinc selenide using an electrochemical iodine cell. Semiconductor Science and Technology **1992**, 7, 464–466.

(79) Van De Walle, C. G.; Laks, D. B.; Neumark, G. F.; Pantelides, S. T. First-principles calculations of solubilities and doping limits: Li, Na, and N in ZnSe. Physical Review B **1993**, 47, 9425–9434.

(80) Ueno, K.; Fudetani, T.; Arakawa, Y.; Kobayashi, A.; Ohta, J.; Fujioka, H. Electron transport properties of degenerate n-type GaN prepared by pulsed sputtering. APL Materials **2017**, 5, 126102.

(81) Tsu, R.; Howard, W. E.; Esaki, L. Optical and Electrical Properties and Band Structure of GeTe and SnTe. Physical Review **1968**, 172, 779–788.

(82) Sb2Te3 charge carrier concentration: Datasheet from "PAULING FILE Multinaries Edition – 2012" in SpringerMaterials. `https://materials.springer.com/isp/physical-property/docs/ppp{\_}1bc8778115586bd2ca54f5aebe46fdf8`.

(83) Tenga, A.; Lidin, S.; Belieres, J.-P.; Newman, N.; Wu, Y.; Haeussermann, U. ChemInform Abstract: Metastable Cd 4 Sb 3 : A Complex Structured Intermetallic Compound with Semiconductor Properties. ChemInform **2009**, 40, 15564–15572.

(84) Hrubý, A.; Kubelík, I.; Štourač, L. Electrical conductivity and thermoelectric power of heavily doped P-type CdSb. Czechoslovak Journal of Physics **1965**, 15, 740–746.

(85) Böttger, P. H. M.; Pomrehn, G. S.; Snyder, G. J.; Finstad, T. G. Doping of p-type ZnSb: Single parabolic band model and impurity band conduction. physica status solidi (a) **2011**, 208, 2753–2759.

(86) Irwin, M. D.; Buchholz, D. B.; Hains, A. W.; Chang, R. P. H.; Marks, T. J. p-Type semiconducting nickel oxide as an efficiency-enhancing anode interfacial layer in polymer bulk-heterojunction solar cells. Proceedings of the National Academy of Sciences **2008**, 105, 2783–2787.

(87) Sato, H.; Minami, T.; Takata, S.; Yamada, T. Transparent conducting p-type NiO thin films prepared by magnetron sputtering. Thin Solid Films **1993**, 236, 27–31.

(88) Newman, R.; Chrenko, R. M. Optical Properties of Nickel Oxide. Physical Review **1959**, 114, 1507–1513.

(89) Chen, C.; Bobela, D. C.; Yang, Y.; Lu, S.; Zeng, K.; Ge, C.; Yang, B.; Gao, L.; Zhao, Y.; Beard, M. C.; Tang, J. Characterization of basic physical properties of Sb2Se3 and its relevance for photovoltaics. Frontiers of Optoelectronics **2017**, 10, 18–30.

(90) Liu, X.; Chen, J.; Luo, M.; Leng, M.; Xia, Z.; Zhou, Y.; Qin, S.; Xue, D.-J.; Lv, L.; Huang, H.; Niu, D.; Tang, J. Thermal Evaporation and Characterization of Sb 2 Se 3 Thin Film for Substrate Sb2Se3 /CdS Solar Cells. ACS Applied Materials & Interfaces **2014**, 6, 10687–10695.

(91) Shay, J. L.; Tell, B.; Buehler, E.; Wernick, J. H. Band Structure of ZnGeP2 and ZnSiP2 - Ternary Compounds with Pseudodirect Energy Gaps. Physical Review Letters **1973**, 30, 983–986.

(92) Bergum, K.; Riise, H. N.; Gorantla, S.; Lindberg, P. F.; Jensen, I. J. T.; Gunnæs, A. E.; Galeckas, A.; Diplas, S.; Svensson, B. G.; Monakhov, E. Improving carrier transport in Cu 2 O thin films by rapid thermal annealing. Journal of Physics: Condensed Matter **2018**, 30, 075702.

(93) Tabuchi, N.; Matsumura, H. Control of Carrier Concentration in Thin Cuprous Oxide Cu 2 O Films by Atomic Hydrogen. Japanese Journal of Applied Physics **2002**, 41, 5060–5063.

(94) Heinemann, M.; Eifert, B.; Heiliger, C. Band structure and phase stability of the copper oxides Cu2O, CuO and Cu4O3. Physical Review B **2013**, 87, 115111.

(95) Ueda, K.; Hosono, H.; Hamada, N. Energy band structure of LaCuOCh (Ch = S, Se and Te) calculated by the full-potential linearized augmented plane-wave method. Journal of Physics: Condensed Matter **2004**, 16, 5179–5186.

(96) Barati, A.; Klein, A.; Jaegermann, W. Deposition and characterization of highly p-type antimony doped ZnTe thin films. Thin Solid Films **2009**, 517, 2149–2152.

(97) Hiramatsu, H.; Ueda, K.; Ohta, H.; Hirano, M.; Kamiya, T.; Hosono, H. Degenerate p-type conductivity in wide-gap LaCuOSSe epitaxial films. Applied Physics Letters **2003**, 82, 1048–1050.

(98) Yang, C.; Kneiβ, M.; Lorenz, M.; Grundmann, M. Room-temperature synthesized copper iodide thin film as degenerate p-type transparent conductor with a boosted figure of merit. Proceedings of the National Academy of Sciences **2016**, 113, 12929–12933.

(99) Ahn, D.; Park, S.-H. Cuprous halides semiconductors as a new means for highly efficient light-emitting diodes. Scientific Reports **2016**, 6, 20718.

(100) Kawazoe, H.; Yasukawa, M.; Hyodo, H.; Kurita, M.; Yanagi, H.; Hosono, H. P-type electrical conduction in transparent thin films of CuAlO2. Nature **1997**, 389, 939–942.

(101) Tate, J.; Ju, H. L.; Moon, J. C.; Zakutayev, A.; Richard, A. P.; Russell, J.; McIntyre, D. H. Physical Review B **2009**, 80, 165206.

(102) Kudo, A.; Yanagi, H.; Hosono, H.; Kawazoe, H. SrCu2O2: A p -type conductive oxide with wide band gap. Applied Physics Letters **1998**, 73, 220–222.

(103) Ohta, H.; Orita, M.; Hirano, M.; Yagi, I.; Ueda, K.; Hosono, H. Electronic structure and optical properties of SrCu2O2. Journal of Applied Physics **2002**, 91, 3074–3078.

(104) Kramida, A.; Ralchenko, Y.; Reader, J.; Team, N. A. NIST Atomic Spectra Database. 2019.

(105) Kittel, C. Introduction to Solid State Physics, 6th ed.; John Wiley & Sons, Inc.: New York, 1986.

(106) Stevanović, V.; Lany, S.; Zhang, X.; Zunger, A. Correcting density functional theory for accurate predictions of compound enthalpies of formation: Fitted elemental-phase reference energies. Physical Review B **2012**, 85, 115104.

(107) Bismuth sulfide (Bi2S3) energy gaps: Datasheet from Landolt-Börnstein. `https://materials.springer.com/lb/docs/sm_lbs_978-3-540-31360-1_936`, Copyright 1998 Springer-Verlag Berlin Heidelberg.

(108) Martinez, L.; Bernechea, M.; De Arquer, F. P. G.; Konstantatos, G. Near IR-sensitive, non-toxic, polymer/nanocrystal solar cells employing Bi 2S 3 as the electron acceptor. Advanced Energy Materials **2011**, 1, 1029–1035.

(109) Bismuth selenide (Bi2Se3) energy gaps: Datasheet from Landolt-Börnstein. `https://materials.springer.com/lb/docs/sm_lbs_978-3-540-31360-1_950`, Copyright 1998 Springer-Verlag Berlin Heidelberg.

(110) Spataru, C. D.; Léonard, F. Fermi-level pinning, charge transfer, and relaxation of spin-momentum locking at metal contacts to topological insulators. Physical Review B **2014**, 90, 085115.

(111) Grüneis, A.; Kresse, G.; Hinuma, Y.; Oba, F. Ionization Potentials of Solids: The Importance of Vertex Corrections. Physical Review Letters **2014**, 112, 096401.

(112) V., B.; M.E., L.; S.L., R.; A., Z. In Properties of Advanced SemiconductorMaterials GaN, AlN, InN, M.E., L., S.L., R., M.S., S., Eds.; John Wiley Sons, Inc.: New York, 2001; pp 1–30.

(113) Lim, K.; Schelhas, L. T.; Siah, S. C.; Brandt, R. E.; Zakutayev, A.; Lany, S.; Gorman, B.; Sun, C. J.; Ginley, D.; Buonassisi, T.; Toney, M. F. The effect of sub-oxide

phases on the transparency of tin-doped gallium oxide. Applied Physics Letters **2016**, 109, 141909.

(114) Irmscher, K.; Naumann, M.; Pietsch, M.; Galazka, Z.; Uecker, R.; Schulz, T.; Schewski, R.; Albrecht, M.; Fornari, R. On the nature and temperature dependence of the fundamental band gap of In2O3. physica status solidi (a) **2014**, 211, 54–58.

(115) Hohmann, M. V.; Ágoston, P.; Wachau, A.; Bayer, T. J. M.; Brötz, J.; Albe, K.; Klein, A. Orientation dependent ionization potential of In 2 O 3 : a natural source for inhomogeneous barrier formation at electrode interfaces in organic electronics. Journal of Physics: Condensed Matter **2011**, 23, 334203.

(116) MgO energy gap: Datasheet from "PAULING FILE Multinaries Edition – 2012" in SpringerMaterials. `https://materials.springer.com/isp/physical-property/docs/ppp_88fc7a6adf40f1c09d4946b62a6ad2ba`, Copyright 2016 Springer-Verlag Berlin Heidelberg & Material Phases Data System (MPDS), Switzerland & National Institute for Materials Science (NIMS), Japan.

(117) Magnesium silicide (Mg2Si) band structure, energy gap: Datasheet from Landolt-Börnstein. `https://materials.springer.com/lb/docs/sm_lbs_978-3-540-31360-1_100`, Copyright 1998 Springer-Verlag Berlin Heidelberg.

(118) Ravich, Y. I.; Efimova, B. A.; Smirnov, I. A. In Semiconducting Lead Chalcogenides; Stil'bans, L. S., Ed.; Springer US: Boston, MA, 1970.

(119) Oman, R. M. Work Function of Lead Sulfide. Journal of Applied Physics **1965**, 36, 2091–2092.

(120) Wang, H.; Gibbs, Z. M.; Takagiwa, Y.; Snyder, G. J. Tuning bands of PbSe for better thermoelectric efficiency. Energy Environ. Sci. **2014**, 7, 804–811.

(121) Varley, J. B.; Schleife, A.; Janotti, A.; Van De Walle, C. G. Ambipolar doping in SnO. Applied Physics Letters **2013**, 103.

(122) Stevanović, V.; Hartman, K.; Jaramillo, R.; Ramanathan, S.; Buonassisi, T.; Graf, P. Variations of ionization potential and electron affinity as a function of surface orientation: The case of orthorhombic SnS. Applied Physics Letters **2014**, 104.

(123) Lany, S. Polymorphism, band-structure, band-lineup, and alloy energetics of the group II oxides and sulfides MgO, ZnO, CdO, MgS, ZnS, CdS. SPIE Photonics West 2014-OPTO: Optoelectronic Devices and Materials. 2014; p 89870K.